Atomic collision cascades on void evolution in vanadium

S. Z. Xu , Z. M. Hao , Y. Q. Su , W. J. Hu , Y. Yu & Q. Wan

Published online: 23 Sep 2011.

Submit your article to this journal

View related articles

Taylor & Francis
Taylor & Francis Group

Atomic collision cascades on void evolution in vanadium

S.Z. Xu[a]*, Z.M. Hao[a], Y.Q. Su[b], W.J. Hu[a], Y. Yu[a] and Q. Wan[a]

[a]*Institute of Structural Mechanics, China Academy of Engineering Physics, Mianyang, People's Republic of China;* [b]*School of Earth and Space Sciences, University of Science and Technology of China, Hefei, People's Republic of China*

Molecular dynamics simulations were performed to study void evolution subject to unidirectional self-bombardment and radiation-induced variation of mechanical properties in single crystalline vanadium. 3D simulation cells of perfect body-centered cubic (BCC) vanadium, as well as those with one, two, four, and six voids, were investigated. For the no void case, the maximum number of defects, maximum volumetric swelling, and the number of defects left in bulk after a sufficiently long recovery period increased with higher primary recoil energy. For the cases containing voids, a primary recoil energy was carefully assigned to an atom so as to initiate a dense collision spike in the voids center, where some self-interstitial atoms gained kinetic energy by secondary replacement collision sequence traveling along the ⟨111⟩ direction. It is found that the larger or the greater the number of voids contained initially in the box, the larger the normalized void volume, and the smaller the volumetric swelling after sufficient recovery of systems. In the single void case, the void became elongated along the bombarding direction; in the multiple void cases, the voids coalesced only when the intervoid ligament distance was short. After sufficient relaxation of the irradiated specimen, a hydrostatic tension was exerted on the box, where the voids were treated as dislocation sources. It is shown that with higher primary recoil energy, the yield stress dropped in cases with smaller or fewer voids but rose in those with larger or greater number of voids. This radiation-induced softening to hardening transition with increasing dislocation density can be attributed to the combined effects of the defect-induced dislocation nucleation and the resistance of defects to dislocation motion. Moreover, as the primary recoil energy increased, the ductility of vanadium in the no void case decreased, but was only slightly changed in the cases containing void.

Keywords: collision cascades; void evolution; softening to hardening transition; single crystalline vanadium; molecular dynamics

1. Introduction

Radiation-induced microstructural evolution in metals is a non-linear function of the initial defect production (*1*). During neutron irradiation, a collision transfers an energy equal to or higher than the threshold value to the primary knock-on atom (PKA), then the PKA is displaced from its original position, which in turn causes additional displacements of other atoms (*2*). With a low energy of the PKA, a Frenkel pair of one vacancy and one self-interstitial atom (SIA) is created in

---

the bulk; at a higher energy, a cascade of atomic collisions appears, leading to the formation and evolution of a more complicated configuration of radiation defects. The recoil energy is initially transferred to atoms by way of replacement collision sequence (RCS); then when the average distance between two consecutive collisions is similar to the first nearest neighbor (1NN) distance of atoms in local lattice sites, most of the cascade energy would be distributed abruptly among the atoms within a spherical region (*3–5*). This process, when accompanied by a low cascade energy, is a dense collision spike, while with a higher energy, it is known as a thermal spike, which can promote local melting, generate a liquid-like region, and continue distributing energy over the bulk (*6*). Generally, a considerable part of the PKA energy is spent on the production of unstable Frenkel pairs and focus on collision sequences which can transfer no mass but energy (*7*). Therefore, the main effect of irradiation is assumed to be the formation of Frenkel pairs, Schottky defects (*8,9*), and clusters of point defects. When no atom with energy above the threshold energy is left, a recovering stage begins, and some vacancies and SIAs recombine, resulting in a final structure of the cascade consisting of a neutral zone with a higher concentration of vacancies and a periphery characterized by SIAs (*2*). According to the conventional theory, the absorption of vacancies and SIAs by radiation-induced extended defects (e.g. void, dislocation, grain boundary) is the main mechanism of recovery of radiation damage. In cases of low irradiation temperature or high dose rates, Dubinko et al. (*7*) considered the non-equilibrium fluctuations of energy of the atoms surrounding extended defects as an additional recovery mechanism.

The buildup and evolution of radiation damage lead to the volumetric swelling of the material (*10*), altering its mechanical properties (*11*). With increasing radiation doses, both experiments (*12–14*) and simulations (*15–17*) showed that the strength (e.g. flow stress, hardness, tensile strength, yield stress) and the ductile–brittle transition temperature of pure metals and their alloys increase, while the ductility (e.g. uniform elongation) and the variation of the mechanical properties decrease (*2*). Byun et al. (*18*) and Li and Zinkle (*19*) developed the deformation and fracture maps of unirradiated and irradiated metals and alloys. The tendency to harden the metals is attributed to the production of defect clusters, which localize the dislocation glide and resist the dislocation motion (*20*). The microscopic mechanisms of this localization include dislocation channeling (*21–23*) and deformation twinning (*24–26*). Thus, much attention was given to the interaction between point defects (or their clusters) and dislocations (*27–29*), twin boundaries (*30–32*), as well as other more general grain boundaries (*33–35*). The migrations of defect clusters (*36–38*) and the interactions among them (*39,40*) were also studied.

The main bulk of the investigations into radiation damage of materials was carried out in or by simulating the fusion reactor environment (*41–43*). In particular, many experiments showed that the vanadium alloys have a low level of long-term neutron activation (*44–46*), low thermal expansion (*47–49*), minimum concentration of undesirable impurities (*50–52*), and satisfactory mechanical properties (*53–55*). Due to these advantages, the vanadium alloys, mainly the V–Cr–Ti system, are best suited for use in self-cooled lithium breeding systems and can provide improved thermodynamic efficiency compared with conventional steel systems (*2*), so they are regarded as promising low activation materials for the first wall and the blanket of fusion reactors, where the average energy of neutron varies from 20 keV to 10 MeV. One can refer to the reviews by Zinkle et al. (*56*) and Muroga et al. (*57*) for the research and development of unirradiated and irradiated vanadium alloys. Therefore, the nanostructural evolutions of vanadium alloys are crucial for the reliability of fusion energy facilities (*58–61*). The authors investigate defects evolution in pure vanadium in this paper, so as to provide a first step forwards the comprehensive analysis of vanadium alloys.

On the one hand, the vacancies in irradiated solids may coalesce into voids (*62–66*), which either move toward dislocation lines or self-organize into a superlattice. The concept of void ordering is based on the mechanisms of both anisotropic interstitial transport (*67,68*) and energy transfer provided by self-focussing breathers (*69*). For common computational treatments of the

nucleation, growth, and coalescence of voids during neutron irradiation of metals, one can refer to (*70*). On the other hand, voids can dissolve into vacancies, and the accompanied shrinkage of voids can promote the volumetric swelling of solids (*71*). Lazarev and Dubinko (*72,73*) studied the radiation-induced void dissolution analytically, and found that this phenomenon in cases of low-temperature or high-dose rate is mainly attributed to vacancy emission from the voids, which can be realized by both thermal fluctuations and collision events near the voids.

Due to the intrinsic difficulty in obtaining information of small length ($\sim$ nm) and time scales ($\sim$ fs) from experiments, numerous *ab initio* calculations (*74–76*) have been performed to investigate the point defects. Using molecular dynamics (MD) simulations, Gibson (*77*) studied the radiation-induced defects in single crystalline Cu as early as 1960, while some later investigations were focussed on radiation damage in vanadium and its alloys (*1,6,78,79*). For larger scales, kinetic Monte Carlo methods (*80–83*) and 3D discrete dislocation dynamics simulations (*84–87*) can provide insight into the microstructural evolution in irradiated materials. At even higher scales, finite-element modeling is being used to study the degradation of mechanical properties of materials under irradiation (*88,89*), for which Wirth et al. (*90*) presented a multiscale modeling methodology. In this paper, the MD method was employed due to its powerful ability to capture the detailed information of radiation damage at both length and time scales of neutron irradiation (*91*). The void evolution subject to self-bombardment in single crystalline vanadium is discussed, and the effects of the primary recoil energy, initial porosity, and number of voids are investigated.

Another phenomenon investigated in our study is the radiation-induced softening of metal, which has not been well analyzed yet. Normally, the radiation damage accumulates in the bulk, resisting the dislocation motion and hardening vanadium and its alloys (*92*). However, in certain conditions, the microhardness of vanadium can be reduced after neutron irradiation (*93*). Thus our study also considers the relationship between dislocation density and the radiation-induced variation of mechanical properties of vanadium. After sufficient recovery of radiation damage, the boxes were deformed under hydrostatic tension, where the voids were treated as dislocation sources. Both the yield stress and ultimate elongation at fracture points were presented and compared with the results from unirradiated vanadium with the same initial arrangement of the voids.

2. Simulation methodology

2.1. *Finnis–Sinclair potential*

The embedded-atom method (EAM) of Daw and Baskes (*94*) has been successfully applied to face-centered cubic (FCC) or nearly filled d-band transition metals and their alloys. However, some BCC transition metals have non-filled d-band (e.g. electron configuration of $[Ar]3d^3 4s^2$ for BCC vanadium), resulting in directional bonding, which disagrees with the premise of an isotropic electron cloud in EAM theory. Finnis and Sinclair (*95*) extended the EAM potential to be more flexible by allowing the atomic density to be environment-dependent (*96*):

$$E_i = F^{t_i}\left[\sum_{j\neq i} \rho^{t_i t_j}(r_{ij})\right] + \frac{1}{2}\sum_{j\neq i} U^{t_i t_j}(r_{ij}), \tag{1}$$

where F is the embedding energy potential of elements t_i and t_j as a function of the local atomic density ρ and U is the interatomic pairwise potential as a function of the separation r_{ij} between atom pairs $\langle ij \rangle$. The Finnis–Sinclair (F–S) potentials are computationally efficient and can provide a robust description of the bonding physics of BCC transition metals (*97*). The vanadium F–S

potential employed in our study is due to Han et al. (*98*). For the extremely short-range repulsion in primary knock-on events, the pairwise potential should be modified by adopting the Biersack–Ziegler form (*99,100*):

$$U(r) = \sum_{k=1}^{6} a_k(r - r_k)^3 H(r_k - r)H(r - r_2)$$

$$+ H(r_2 - r)H(r - r_1)e^{-9.2454+50.1016r+42.5111r^2+10.0263r^3}$$

$$+ H(r_1 - r)\xi\left(\frac{rZ^{1/3}}{0.3311}\right)\frac{Z^2}{r} \tag{2a}$$

$$\xi(x) = 0.1818e^{-3.2x} + 0.5099e^{-0.9423x} + 0.2802e^{-0.4029x} + 0.02817e^{-0.2016x}, \tag{2b}$$

where H is the Heaviside function, Z the nuclear charges of vanadium, a_k and r_k determined in Ref. (*98*). The reliability of this F–S potential, of calculating the lattice parameter, elastic constants, cohesive energy, surface energy, formation and migration energy of vacancy and SIA, has been examined carefully by the authors.

2.2. *MD simulations*

The simulation cell is a 3D single crystal BCC lattice with a lattice constant a_0 of 3.03 Å. The edge length of the cubic box L is $80a_0$; all axes are normal to {100} faces with periodic boundary conditions, so there are about one million atoms in the cell. After sufficient relaxation at 300 K, a primary recoil energy E_{pka} from 2 to 40 keV was given to an atom (i.e. the PKA) near the middle of the box. In this way, the PKA was assigned a certain velocity in the [110] direction, along which the threshold displacement energy is the highest (*101*), such that the number of defects crossing the boundaries can be reduced as much as possible. The classical equations of motion were integrated using Verlet algorithm by LAMMPS (*102*), with the time step of 0.01 fs for the first 2 ps, then 0.1 fs for another 8 ps, and 1 fs for the last 10 ps. A Nosé–Hoover thermostat (*103,104*) was applied to obtain an NPT ensemble with a constant temperature of 300 K and a pressure of 0 Pa.

A dense collision spike were observed in all cases with no initial voids. During this spike, some atoms acquired velocities in the close-packed directions ⟨111⟩ from the interaction with their surroundings, leading to several secondary RCSs. By tracking these atoms backwards along their trajectories, all these secondary RCSs were found to be initiated from the same point. We refer this point as the center of dense collision spike, and the distance between which and the initial position of the PKA is denoted as L_0. In the cases containing voids, the voids were created near the box center, and E_{pka} was assigned to an atom whose distance from box center along the [110] direction was L_0, so that the dense collision spike could be initiated in the voids center. Details of the arrangement of the voids can be found in Figure 1.

The authors performed MD simulations for as long as 100 ps after the initial bombardment, showing that 20 ps is sufficient for the system to relax after irradiation of E_{pka} applied in this paper. Then a hydrostatic tension was exerted on the box with a strain rate of $5 \times 10^8 \, s^{-1}$. The strain-controlled simulations were realized by the Parrinello–Rahman method (*105*) with the time step of 1 fs, and the virial definition of atomic level stress without the kinetic portion (*106*) was employed to calculate the hydrostatic stress of system σ_h:

$$\sigma_h = \frac{1}{3}\sum_{\alpha}\sigma_{\alpha\alpha} = -\frac{1}{V}\left(\sum_i \sum_{j>i} r_{ij}^{\alpha} f_{ij}^{\alpha}\right), \tag{3}$$
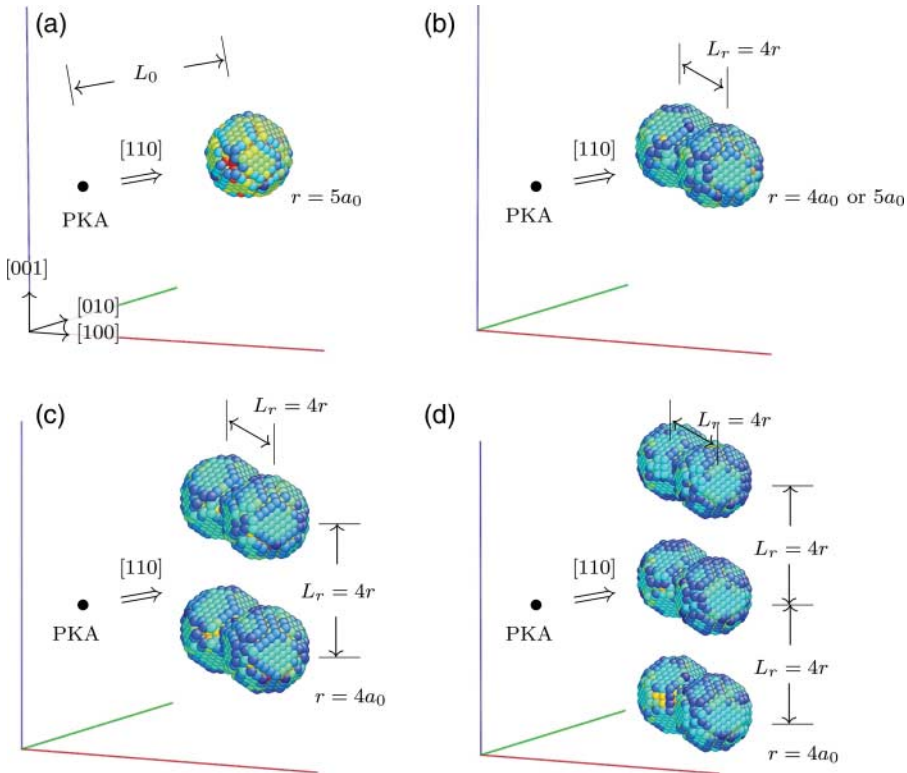
Figure 1.   Illustrations of the arrangement of voids in the cases which contain (a) one, (b) two, (c) four, and (d) six voids. The PKA was assigned a velocity along the [110] direction toward the center of a single void or a void group. L_0 is the distance between the initial position of the PKA and the dense collision spike center for the no void case. L_r is the distance between the centers of adjacent voids. Note that in the two-void cases, the void radius r of both $4a_0$ and $5a_0$ were introduced to study the effects of initial porosity.

where f is the interatomic force, α the Cartesian coordinates, and V the Voronoi volume of the specimen.

The atomic configurations were colored by centrosymmetry parameter (CSP) implemented in AtomEye (*107*):

$$c_i = \frac{\sum_{l=1}^{k/2} D_l}{2 \sum_{j=1}^{k} |\vec{R}_j|^2},   \tag{4}$$

where c_i is the CSP of atom i, k the number of opposite neighbor pairs, and the function $D_l = |\vec{R}_l + \vec{R}_{l'}|^2$ minimized by bond vector $\vec{R}_{l'}$. c_i is dimensionless with a maximum value of 1. Seven pairs within the 2NN shell in a perfect BCC lattice were summed over, which has been proved to be less noisy than summing over the four pairs within the 1NN shell (*97*). To highlight the void surface and dislocations, only atoms with $c_i \geq 0.01$ are made visible in the snapshots.

Specifically, the point defects were distinguished by dividing the box into a number of Wigner–Seitz cells. If there are no atoms inside a cell, the cell corresponds to a vacancy; if two or more atoms occupy a cell, then SIAs are believed to form here. The MD simulations of atomic displacement cascades in BCC Fe confirmed that this method is valid for estimating the number of Frenkel pairs (*108*).

3. Results and discussion

3.1. *Atomic displacement cascades in perfect vanadium*

It can be seen from Figure 2 that as E_{pka} increased, the distance between the initial position of the PKA and dense collision spike center decreased. This is due to the splitting of the main cascade into increasing number of subcascades initiated by an increasing number of secondary knock-on atoms (SKAs) in cases with higher E_{pka}. Consequently, there is a smaller distance between consecutive collisions of SKAs which shortens the distance they need to travel before the dense collision spike is initiated.

The evolution of the number of point defects versus E_{pka} is depicted in Figure 3. After the initial bombardment, the number of point defects rises rapidly, and after a short time, denoted as the peak time t_p, it reaches a maximum n_{dmax}. In the following recovery stage, the system cools down, and the unstable Frenkel pairs recombine, until the number of defects reduces to a relatively stable value n_{drec}. These data calculated by the present MD simulations are close to those given out by Psakhie et al. (*6*) using another F–S potential. Both the maximum number of defects and the corresponding time grew linearly with E_{pka}. Moreover, as E_{pka} increased, more defects were left after a sufficiently long recovery period, but the variation decreased (Figure 3(d)). This is because in cases of higher E_{pka}, more SIAs were created during the dense collision spike, crossing the boundary and recombining with vacancies at the other end. In addition, since the creation of defects led to the volumetric swelling of irradiated vanadium, the evolution of system swelling versus E_{pka} was similar to that of number of defects (Figure 4).

Several secondary RCSs along the $\langle 111 \rangle$ direction are presented in Figure 5(b). The longest average distance the secondary RCS traveled corresponded to the maximum number of defects. The locally disordered region caused by the dense collision spike was rapidly quenched to form a damaged, amorphous, solid structure. This structure mainly consisted of vacancy clusters, with which the SIAs brought about by the secondary RCS were difficult to recombine, even after sufficient recovery of system at 300 K. The most stable configuration of SIAs here is found to be $\langle 111 \rangle$-split dumbbell, which agrees with the results of both first principle calculations (*109*) and MD simulations (*98*). Zepeda-Ruiz et al. (*101,110,111*) also showed that the $\langle 111 \rangle$
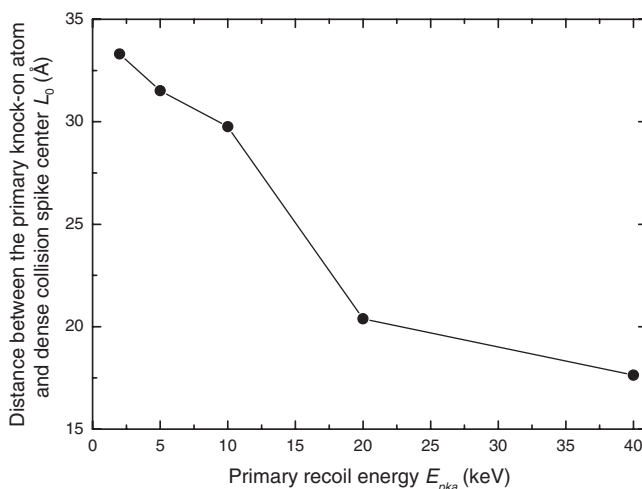
Figure 2. The distance between the initial position of the PKA and dense collision spike center L_0 versus the primary recoil energy E_{pka}.
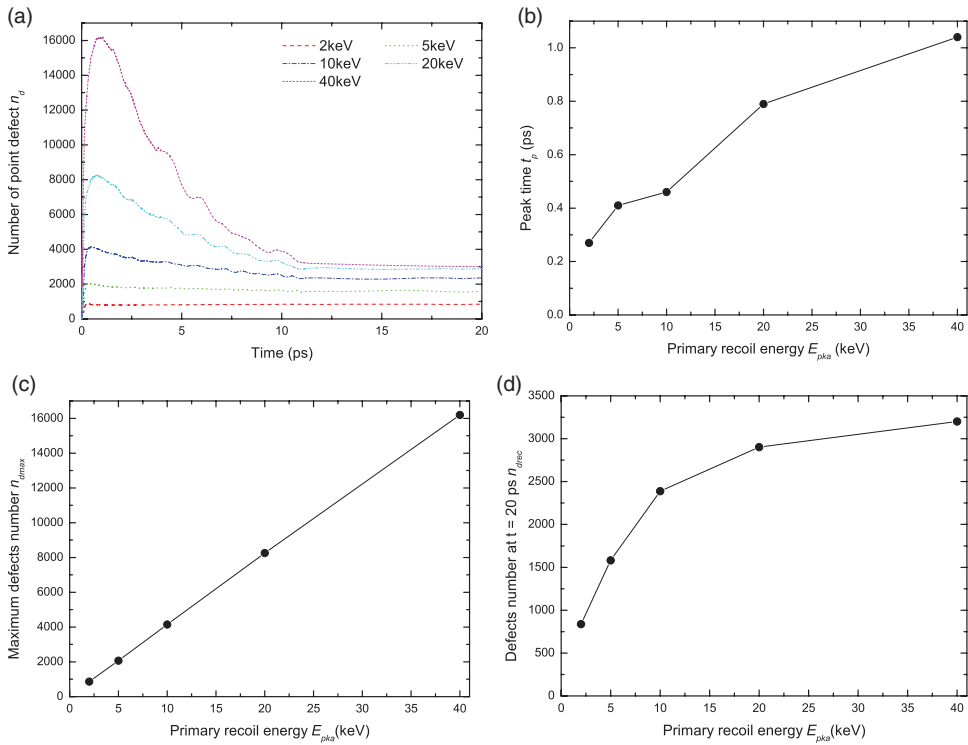
Figure 3. (a) Evolution of number of defects n_d in cases of different primary recoil energies E_{pka}. (b–d) Peak time t_p, maximum number of defects n_{dmax}, and the number of defects after a sufficiently long recovery period n_{drec} versus E_{pka}, respectively.
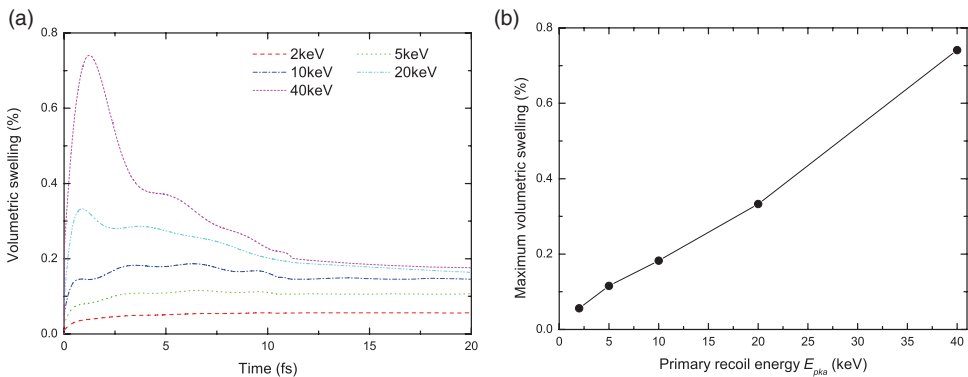
Figure 4. (a) Evolution of volumetric swelling in cases of different primary recoil energies E_{pka}. (b) The maximum system swelling versus E_{pka}.

dumbbell configuration is stable relative to other dumbbell orientations. These studies disputed the earlier predictions that the $\langle 100 \rangle$ (*112*) or $\langle 110 \rangle$ (*1,113,114*) configuration was the most stable. In addition, the Frenkel pairs and dislocation loops were observed near the dense collision spike center, where the loop was formed by four segments on (110), ($\bar{1}$10), and (101) planes (Figure 5(d)).
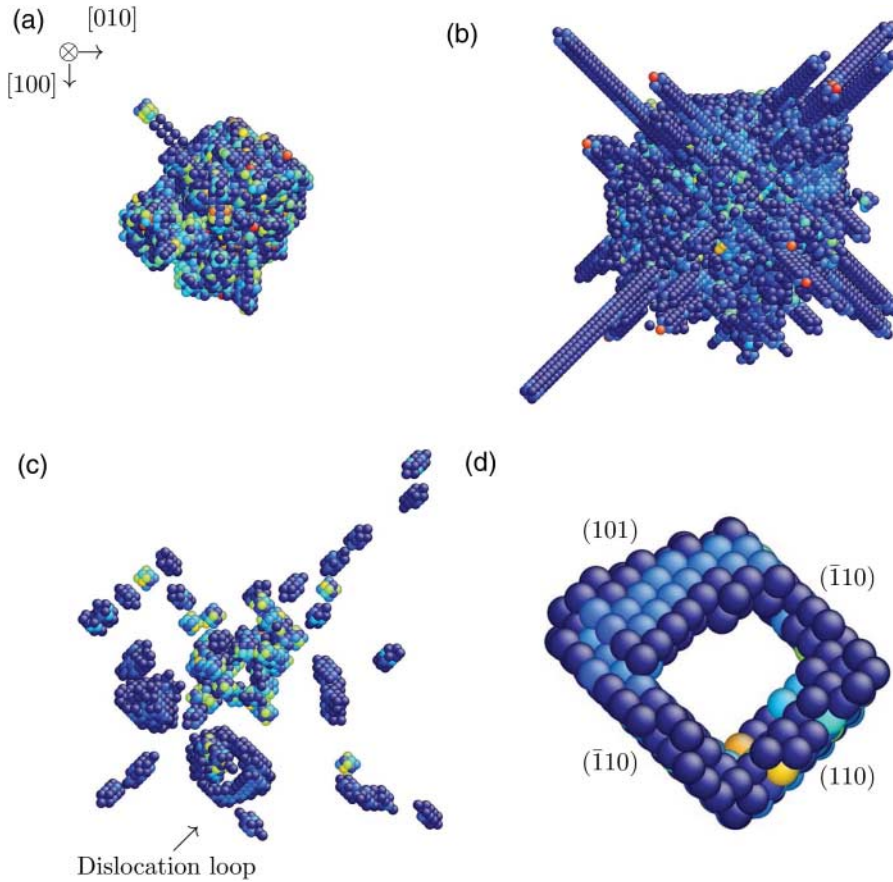
Figure 5.   Snapshots from MD simulations of a specimen subject to neutron irradiation at (a) 100 fs, (b) 400 fs, and (c) 20 ps after the initial bombardment. Some atoms acquired velocities in the close-packed directions $\langle 111 \rangle$ from the interaction with their surroundings, leading to several secondary RCSs. After sufficient recovery of the system, the most stable configuration of SIAs was $\langle 111 \rangle$-split dumbbell. (d) A dislocation loop, formed by four segments on (110), ($\bar{1}$10), and (101) planes, is observed in the vicinity of the dense collision spike center after sufficient recovery.

3.2.   *Void evolution under unidirectional bombardment*

The void volume and volumetric swelling of the specimen at $t = 20$ ps are presented versus E_{pka} in Figure 6. The void volume was calculated in this way: first, the volume of all vacancies were summed up; secondly, the volume of vacancies and vacancy clusters with fewer than 30 vacancies were deducted (the maximum vacancy cluster in vanadium contains 22 vacancies under $E_{pka} = 10$ keV according to (6)); finally, the remaining volume was normalized by the initial void volume in each case. The void shrank under bombardment by its dissolution into vacancies, which migrated into the bulk and promoted the volumetric swelling. Thus, in each case, the higher the E_{pka}, the smaller the void volume left, and the larger the volumetric swelling. The only exception in targets containing voids was that the swelling under $E_{pka} = 40$ keV is smaller than that under $E_{pka} = 20$ keV. This is because when $E_{pka} = 40$ keV, some SIAs crossed the periodic boundary and re-entered the specimen at the other side, so they were recombined with the vacancies emitted from the voids. In addition, since the center of dense collision spike coincided with that of the voids, only the part of voids surface near the center can emit vacancies, while the other parts, which were not bombarded directly, absorbed vacancies instead due to their higher surface energy.
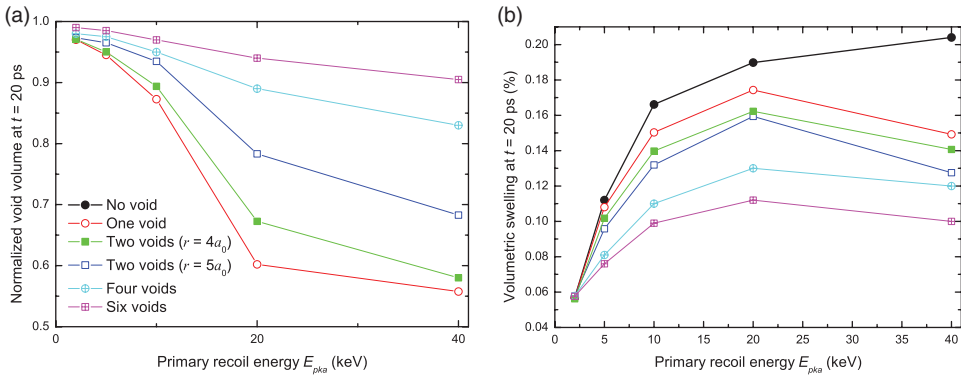
Figure 6.   (a) The void volumes, which are normalized by the initial void volume in each case containing voids, versus primary recoil energy E_{pka}. (b) The volumetric swelling of the specimens in cases of different E_{pka}. All were calculated at $t = 20$ ps.

Therefore, the void shrinkage and induced swelling were reduced with increasing void volume, even in cases with the same number of voids. It is also noteworthy that the number of voids influenced the accumulation of radiation damage, e.g. the initial void volume in the single void case with $r = 5a_0$ and the two-void case with $r = 4a_0$ was very close, yet the void shrinkage and system swelling were smaller in the latter case. This phenomenon can be attributed to the arrangement of the voids: in the one void case, the RCS initiated by the PKA traveled directly toward the void; in the multiple-void cases, it was the secondary RCS, which carried much less energy than the initial RCS, that resulted in the vacancies emission.

The snapshots of the void evolution under irradiation are shown in Figure 7. In the single void case, the void became elongated along the bombarding direction; in the two-void cases, the voids with $r = 4a_0$ coalesced while those with $r = 5a_0$ did not, and neither did voids in cases with four and six voids because of the longer intervoid ligament distance in the last three cases. The simulations of void and helium bubble stability in silicon by Okuniewski et al. (*115*) suggested that the void collapses completely under isotropic xenon bombardment, but becomes elongated and resists closure under unidirectional irradiation.

3.3.   *Radiation-induced softening to hardening transition*

Under hydrostatic tension, the yield strength of the material was found from the plastic deformation caused by the nucleation of dislocations. In the case with no initial void, the screw dislocation along $\langle 111 \rangle$ split on three non-planar $\{110\}$ planes; in the cases containing voids, the dislocations were emitted from the void surface. The hydrostatic stress at the yield point, which was denoted by the breakdown of the linear relationship between stress and strain, is shown in Figure 8(a). It is found that under the same E_{pka}, the yield stress was lower in cases with larger or greater number of voids, except that when $E_{pka} = 40$ keV, σ_Y was higher in the two-void case with $r = 4a_0$ than in the single void case. This exception is due to the coalescence of the two voids in the dense collision spike, which resulted in a void smaller than that of the single void case. Radiation-induced softening of vanadium (i.e. decreasing yield stress) was observed in the cases of no initial void, one void and two voids with $r = 4a_0$. However, in cases of larger or greater number of voids, the hardening of vanadium by irradiation began to be more pronounced, which agrees with experiments by Schiraishi et al. (*116*). This radiation-induced softening to hardening transition (SHT) is of interest. On the one hand, the interlocking of dislocations at defects strengthened the vanadium; on the other hand, the defects themselves emitted dislocations, and so the required
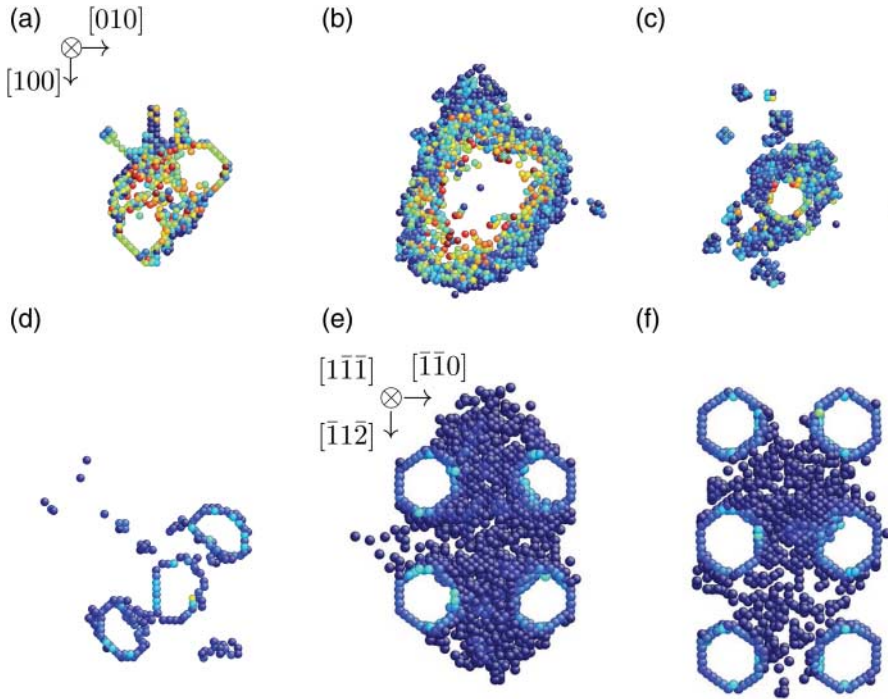
Figure 7. Snapshots of voids coalescence in the two-void case with $r = 4a_0$, at (a) 80 fs, (b) 800 fs, and (c) 20 ps, respectively; snapshots of the (d) two-void case with $r = 5a_0$, (e) four voids, and (f) six voids cases, where voids did not coalesce.
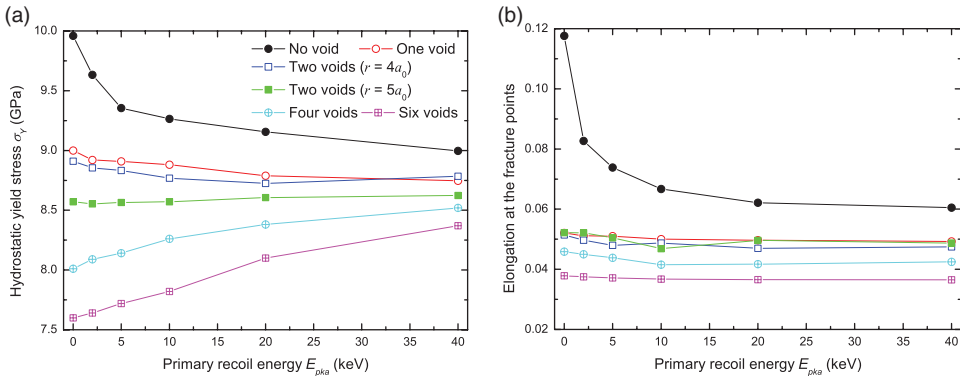
Figure 8. (a) The hydrostatic yield stress σ_Y in each case versus primary recoil energy E_{pka}. (b) The total elongation of the box at the fracture points along each axis in each case versus E_{pka}.

stress for plasticity was much smaller than that needed in defect-free crystals (*117*). Therefore, when the volume or number of voids is increased, the combined effects of these two contradictory mechanisms lead to the transition from radiation-induced softening to hardening as the resistance of defects to dislocation motion is intensified (Figure 9).

The elongation of the box along each axis at the fracture points is shown in Figure 8(b). It can be seen from the case with no initial void that the ductility of vanadium decreased as E_{pka} increased. However, for the cases containing voids, the ductility seemed to be unaffected by irradiation, except that the ductility of unirradiated vanadium was slightly higher than that of the irradiated

S.Z. Xu et al.
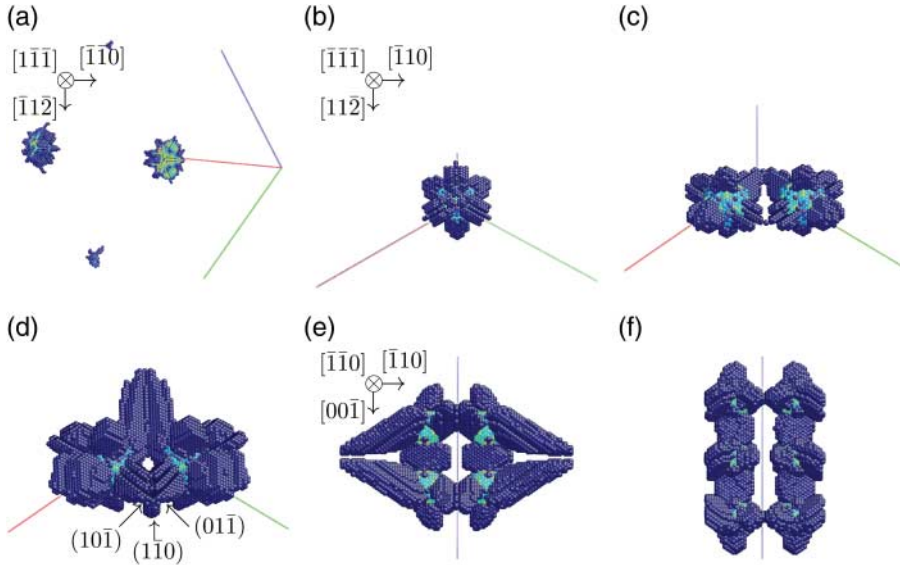
Figure 9.   Snapshots of dislocation emission at the yield points for unirradiated vanadium in the (a) no void case, (b) single void case, (c–d) two-void case, (e) four-void case, and (f) six-void case. Note that the dislocation density increased with the growing number of initial voids.

one, showing that the resisted motion of dislocations caused by voids was much stronger than that caused by vacancies and SIAs. Moreover, the cases with larger or greater number of initial voids were accompanied by lower ductility of vanadium under the same E_{pka}.

4.   Conclusions

In this paper, MD simulations were performed using the F–S potential to study spherical void evolution subject to neutron irradiation in single crystalline vanadium. The radiation induced variation of mechanical properties of vanadium was also investigated. The results obtained are summarized as follows:

(1) As is well known, the neutron irradiation in metals will induce the radiation damage of vacancies, SIAs, and dislocation loops. These three defects, as well as the relevant volumetric swelling of system, were also discovered in the present study. In perfect vanadium, the number of defects rose sharply after initial bombardment, and then reduced during the recovery stage to a relatively stable value. The maximum number of defects, the peak time, and the number of defects left after a sufficient recovery period increased under higher primary recoil energy, and so did the maximum volumetric swelling of the specimen.

(2) During the dense collision spike, some atoms acquired velocities along the ⟨111⟩ direction. The results that the ⟨111⟩-split dumbbell was the most stable configuration of SIAs after sufficient recovery time disputed the earlier predictions by rough empirical potentials and agreed well with more recent calculations by an accurate *ab initio* method. The Frenkel pairs and dislocation loops were also observed near the dense collision spike center.

(3) As the single void in amorphous silicon in (*115*), the single void in vanadium became elongated along the bombarding direction. Besides, the arrangements of the multiple voids were set up, such that the center of the dense collision spike concurred with that of the void group. Using these configurations, it is realized for the first time, to the authors' knowledge that the dense

collision spike during irradiation coalesces the adjacent voids with a short intervoid ligament distance; in cases with a longer ligament distance, the voids did not coalesce for the same primary recoil energy. It is also found that the higher the primary recoil energy, the smaller the void volume left, and the larger the volumetric swelling of the specimen.

(4) For the relaxed specimen subject to hydrostatic tension, when the primary recoil energy increased, the yield stress dropped in perfect vanadium, as well as the cases of one void and two voids with a small radius. However, the yield stress rose in cases with larger or greater number of voids, i.e. higher dislocation density at the threshold of plasticity. This radiation-induced SHT of metal was found in previous experiments but the mechanism has not been understood thoroughly. In this paper, such transition was attributed to the combined effects of the defect-induced dislocation nucleation and the resistance of defects to dislocation motion. Moreover, the ductility of vanadium in the no void case decreased, but was only slightly changed with varying primary recoil energy in cases containing voids.

Acknowledgements

References

(1) Morishita, K.; Díaz de la Rubia, T. In *A Molecular Dynamics Simulation Study of Defect Production in Vanadium*, Proceedings of Ion Solid Interaction for Material Modification and Processing Symposium, Boston, MA, 1996; pp 39–44.
(2) Ivanov, L.I.; Platov, Y.M. *Radiation Physics of Metals and its Applications*; Cambridge International Science Publishing Ltd: Cambridge, UK, 2004.
(3) Marks, N.A.; Thomas, B.S.; Smith, K.L.; Lumpkin, G.R. *Nucl. Instrum. Methods Phys. Res. B* **2008,** *266,* 2665–2670.
(4) Meftah, A.; Brisard, F.; Costantini, J.M.; Dooryhee, E.; Hage-Ali, M.; Hervieu, M.; Stoquert, J.P.; Studer, F.; Toulemonde, M. *Phys. Rev. B* **1994,** *49,* 12457–12463.
(5) Díaz de la Rubia, T.; Averback, R.S.; Hsieh, H.; Benedek, R. *J. Mater. Res.* **1989,** *4,* 579–586.
(6) Psakhie, S.G.; Zolnikov, K.P.; Kryzhevich, D.S.; Zheleznyakov, A.V.; Chernov, V.M. *Phys. Mesomech.* **2009,** *12,* 20–28.
(7) Dubinko, V.I.; Klepikov, V.F. *J. Nucl. Mater.* **2007,** *362,* 146–151.
(8) Dubinko, V.I. [Online]; 2002. arXiv:cond-mat/0212154v1 (accessed Jan 5, 2011).
(9) Dubinko, V.I.; Vainshtein, D.I.; Den Hartog, H.W. *Radiat. Eff. Def. Solids* **2003,** *158,* 705–719.
(10) Cottrell, G.A. *Fusion Eng. Des.* **2003,** *66–68,* 253–257.
(11) Dubinko, V.I. *J. Nucl. Mater.* **1995,** *225,* 26–32.
(12) Plantz, D.H.; Dodd, R.A.; Kulcinski, G.L. *Metall. Trans. A* **1989,** *20A,* 2689–2693.
(13) Kluch, R.L.; Maziasz, P.J. *J. Nucl. Mater.* **1992,** *187,* 43–54.
(14) Oliver, W.C.; McHargue, C.J.; Zinkle, S.J. *Thin Solids Films* **1987,** *153,* 185–196.
(15) Terdalkar, S.S.; Zhang, S.L.; Rencis, J.J.; Hsia, K.J. *Int. J. Solids Struct.* **2008,** *45,* 3908–3917.
(16) Shim, J.H.; Lee, H.J.; Wirth, B.D. *J. Nucl. Mater.* **2006,** *351,* 56–64.
(17) Ma, Y.; Chen, Y.X.; Zhou, Y.C. *Radiat. Eff. Def. Solids* **2008,** *163,* 189–197.
(18) Byun, T.S.; Hashimoto, N.; Farrell, K. *J. Nucl. Mater.* **2006,** *351,* 303–315.
(19) Li, M.M.; Zinkle, S.J. *J. Nucl. Mater.* **2007,** *361,* 192–205.
(20) Byun, T.S.; Hashimoto, N.; Farrell, K.; Lee, E.H. *J. Nucl. Mater.* **2006,** *349,* 251–264.
(21) Bailat, C.; Almazouzi, A.; Baluc, N.; Schäublin, R.; Gröschel, F.; Victoria, M. *J. Nucl. Mater.* **2000,** *283–287,* 446–450.
(22) Hashimoto, N.; Byun, T.S.; Farrell, K.; Zinkle, S.J. *J. Nucl. Mater.* **2005,** *336,* 225–232.
(23) Hashimoto, N.; Byun, T.S.; Farrell, K.; Zinkle, S.J. *J. Nucl. Mater.* **2004,** *329–333,* 947–952.
(24) Lee, E.H.; Byun, T.S.; Hunn, J.D.; Yoo, M.H.; Farrell, K.; Mansur, L.K. *Acta Mater.* **2001,** *49,* 3269–3276.
(25) Lee, E.H.; Yoo, M.H.; Byun, T.S.; Hunn, J.D.; Farrell, K.; Mansur, L.K. *Acta Mater.* **2001,** *49,* 3277–3287.
(26) Byun, T.S.; Lee, E.H.; Hunn, J.D. *J. Nucl. Mater.* **2003,** *321,* 29–39.
(27) Osersky, Yu.N.; Bacon, D.J. *J. Nucl. Mater.* **2003,** *323,* 268–280.
(28) Rodney, D.; Martin, G.; Bréchet, Y. *Mater. Sci. Eng. A* **2001,** *309–310,* 198–202.
(29) Wen, M.; Takahashi, A.; Ghoniem, N.M. *J. Nucl. Mater.* **2009,** *392,* 386–395.
(30) Hussain, F.; Hayat, S.S.; Imran, M. *Phys. B* **2011,** *406,* 1060–1064.

(31) de Diego, N.; Bacon, D.J. *J. Nucl. Mater.* **1993,** *203,* 1–9.
(32) Ingle, K.W.; Bristowe, P.D.; Crocker, A.G. *Philos. Mag.* **1976,** *33,* 663–674.
(33) Pérez-Pérez, F.J.; Smith, R. *Nucl. Instrum. Methods Phys. Res. B* **2000,** *164,* 487–494.
(34) Terentyev, D.; He, X. *Comput. Mater. Sci.* **2010,** *50,* 925–933.
(35) Tschopp, M.A.; Horstemeyer, M.F.; Gao, F.; Sun, X.; Khaleel, M. *Scripta Mater.* **2011,** *64,* 908–911.
(36) Chiesa, S.; Derlet, P.M.; Dudarev, S.L. *Phys. Rev. B* **2009,** *79,* 214109.
(37) Marian, J.; Wirth, B.D.; Caro, A.; Sadigh, B.; Odette, G.R.; Perlado, J.M.; Díaz de la Rubia, T. *Phys. Rev. B* **2002,** *65,* 144102.
(38) Hu, S.Y.; Henager, C.H., Jr. *Acta Mater.* **2010,** *58,* 3230–3237.
(39) Pelfort, M.; Osetsky, Yu.N.; Serra, A. *Philos. Mag. Lett.* **2001,** *81,* 803–811.
(40) Tang, M.J.; Colombo, L.; Zhu, J. *Phys. Rev. B* **1997,** *55,* 14279–14289.
(41) Dudarev, S.L.; Boutard, J.L.; Lässer, R.; Caturla, M.J.; Derlet, P.M.; Fivel, M.; Fu, C.C.; Lavrentiev, M.Y.; Malerba, L.; Mrovec, M.; Nguyen-Manh, D.; Nordlund, K.; Perlado, M.; Schäublin, S.; Van Swygenhoven, H.; Terentyev, D.; Wallenius, J.; Weygand, D.; Willaime, F. *J. Nucl. Mater.* **2009,** *386–388,* 1–7.
(42) Fabritsiev, S.A.; Zinkle, S.J.; Singh, B.N. *J. Nucl. Mater.* **1996,** *233–237,* 127–137.
(43) Muroga, T.; Nagasaka, T.; Iiyoshi, A.; Kawabata, A.; Sakurai, S.; Sakata, M. *J. Nucl. Mater.* **2000,** *283–287,* 711–715.
(44) Fukumoto, K.; Matsui, H.; Muroga, T.; Zinkle, S.J.; Hoelzer, D.T.; Snead, L.L. *J. Nucl. Mater.* **2004,** *329–333,* 472–476.
(45) Kameda, J.; Bloomer, T.E.; Lyu, D.Y. *J. Nucl. Mater.* **1998,** *258–263,* 1482–1486.
(46) Chen, C.C.; Arsenault, R.J. *Metall. Trans. A* **1976,** *7A,* 55–61.
(47) Li, H.X.; Hamilton, M.L.; Jones, R.H. *Scripta Metall. Mater.* **1995,** *33,* 1063–1068.
(48) Koyama, M.; Fukumoto, K.; Matsui, H. *J. Nucl. Mater.* **2004,** *329–333,* 442–446.
(49) Iwai, T.; Sekimura, N.; Garner, F.A. *J. Nucl. Mater.* **1996,** *239,* 157–161.
(50) Lyakishev, N.P.; Dyomina, E.V.; Ivanov, L.I.; Kolotov, V.P.; Kashin, V.I.; Platov, Yu.; Savvateev, N.N.; Vinogradova, N.A. *J. Nucl. Mater.* **1996,** *233–237,* 1516–1522.
(51) Tamura, T.; Yominaga, Y.; Matsumoto, K.; Fuda, T.; Kuriiwa, T.; Kamegawa, A.; Takamura, H.; Okada, M. *J. Alloys Compd.* **2002,** *330–332,* 522–525.
(52) Kuriiwa, T.; Tamura, T.; Amemiya, T.; Fuda, T.; Kamegawa, A.; Takamura, H.; Okada, M. *J. Alloys Compd.* **1999,** *293–295,* 433–436.
(53) Ivanov, L.I.; Ivanov, V.V.; Lazorenko, V.M.; Platov, Yu.M.; Tovtin, V.I.; Toropova, L.S. *J. Nucl. Mater.* **1992,** *191–194,* 1075–1079.
(54) Li, H.X.; Jones, R.H.; Hirth, J.P. *Scripta Metall. Mater.* **1995,** *32,* 611–616.
(55) Gan, Y.X.; Aglan, H.A.; Steward, R.V. *J. Nucl. Mater.* **2001,** *299,* 157–164.
(56) Zinkle, S.J.; Matsui, H.; Smith, D.L.; Rowcliffe, A.F.; van Osch, E.; Abe, K.; Kazakov, V.A. *J. Nucl. Mater.* **1998,** *258–263,* 205–214.
(57) Muroga, T.; Nagasaka, T.; Abe, K.; Chernov, V.M.; Matsui, H.; Smith, D.L.; Xu, Z.Y.; Zinkle, S.J. *J. Nucl. Mater.* **2002,** *307–311,* 547–554.
(58) Satou, M.; Yip, S.; Abe, K. *J. Nucl. Mater.* **2002,** *307–311,* 1007–1010.
(59) Morishita, K.; Díaz de la Rubia, T., Alonso, E.; Sekimura, N.; Yoshida, N. *J. Nucl. Mater.* **2002,** *283–287,* 753–757.
(60) Morishita, K.; Díaz de la Rubia, T. *J. Nucl. Mater.* **1999,** *271–272,* 35–40.
(61) Morishita, K.; Sekimura, N.; Díaz de la Rubia, T. *J. Nucl. Mater.* **1997,** *248,* 400–404.
(62) Shimomura, Y.; Mukouda, I.; Sugio, K. *J. Nucl. Mater.* **1997,** *251,* 61–71.
(63) Yu, H.C.; Lu, W. *Acta Mater.* **2005,** *53,* 1799–1807.
(64) Evans, J.H. *Philos. Mag.* **2006,** *86,* 173–188.
(65) Rokkam, S.; El-Azab, A.; Millett, P.; Wolf, D. *Modell. Simul. Mater. Sci. Eng.* **2009,** *17,* 064002.
(66) Vainshtein, D.I.; Dubinko, V.I.; Turkin, A.A.; den Hartog, H.W. *Nucl. Instrum. Methods Phys. Res. B* **2000,** *166–167,* 550–555.
(67) Semenov, A.A.; Woo, C.H.; Frank, W. *Appl. Phys. A* **2008,** *93,* 365–377.
(68) Semenov, A.A.; Woo, C.H. *Phys. Rev. B* **2006,** *74,* 024108.
(69) Dubinko, V. *Nucl. Instrum. Methods Phys. Res. B* **2009,** *267,* 2976–2979.
(70) Surh, M.P.; Sturgeon, J.B.; Wolfer, W.G. *J. Nucl. Mater.* **2008,** *378,* 86–97.
(71) Dubinko, V.I.; Guglya, A.G.; Melnichenko, E.; Vasilenko, R. *J. Nucl. Mater.* **2009,** *385,* 228–230.
(72) Lazarev, N.P.; Dubinko, V.I. *Radiat. Eff. Def. Solids* **2003,** *158,* 803–810.
(73) Dubinko, V.I.; Lazarev, N.P. *Nucl. Instrum. Methods Phys. Res. B* **2005,** *228,* 187–192.
(74) Nagasako, N.; Jahnátek, M.; Asahi, R.; Hafner, J. *Phys. Rev. B* **2010,** *81,* 094108.
(75) Li, S.; Alemany, M.M.G.; Chelikowsky, G.R. *J. Chem. Phys.* **2004,** *121,* 5893–5898.
(76) Louis, C.N.; Iyakutti, K. *Phys. Rev. B* **2003,** *67,* 094509.
(77) Gibson, J.B.; Goland, A.N.; Milgram, M.; Vineyard, G.H. *Phys. Rev.* **1960,** *120,* 1229–1253.
(78) Sorkin, V.; Polturak, E.; Adler, J. *Phys. Rev. B* **2003,** *68,* 174102.
(79) Sorkin, V.; Polturak, E.; Adler, J. *Phys. Rev. B* **2003,** *68,* 174103.
(80) Alonso, E.; Caturla, M.J.; Díaz de la Rubia, T.; Perlado, J.M. *J. Nucl. Mater.* **2000,** *276,* 221–229.
(81) Heinisch, H.L.; Singh, B.N.; Golubov, S.I. *J. Nucl. Mater.* **2000,** *276,* 59–64.
(82) Caturla, M.J.; Soneda, N.; Alonso, E.; Wirth, B.D.; Díaz de la Rubia, T.; Perlado, J.M. *J. Nucl. Mater.* **2000,** *276,* 13–21.
(83) Trinkaus, H.; Heinisch, H.L.; Barashev, A.V.; Golubov, S.I.; Singh, B.N. *Phys. Rev. B* **2002,** *66,* 060105.

(84) Ghoniem, N.M.; Tong, S.H.; Huang, J.; Singh, B.N.; Wen, M. *J. Nucl. Mater.* **2002,** *307–311,* 843–851.

(85) Díaz de la Rubia, T.; Zbib, H.M.; Khraishi, T.A.; Wirth, B.D.; Victoria, M.; Caturla, M.J. *Nature* **2000,** *406,* 871–874.

(86) Ghoniem, N.M.; Singh, B.N.; Sun, L.Z.; Díaz de la Rubia, T. *J. Nucl. Mater.* **2000,** *276,* 166–177.

(87) Sun, L.Z.; Ghoniem, N.M.; Tong, S.H.; Singh, B.N. *J. Nucl. Mater.* **2000,** *283–287,* 741–745.

(88) Odette, G.R.; He, M.Y.; Donahue, E.G.; Spätig, P.; Yamamoto, T. *J. Nucl. Mater.* **2002,** *307–311,* 171–178.

(89) Odette, G.R.; He, M.Y. *J. Nucl. Mater.* **2002,** *307–311,* 1624–1628.

(90) Wirth, B.D.; Caturla, M.J.; Díaz de la Rubia, T.; Zbib, H. *Nucl. Instrum. Methods Phys. Res. B* **2001,** *180,* 23–31.

(91) Glosli, J.; Graziani, F.; More, R.; Murillo, M.; Streitz, F.; Surh, M. *J. Phys. A: Math. Theo.* **2009,** *42,* 214030.

(92) van Osch, E.V.; de Vries, M.I. *J. Nucl. Mater.* **1999,** *271–272,* 162–166.

(93) Ivanov, L.I.; Ivanov, V.V.; Lazorenko, V.M.; Platov, Yu.M.; Tovtin, V.I. *J. Nucl. Mater.* **1992,** *191–194,* 928–932.

(94) Daw, M.S.; Baskes, M.I. *Phys. Rev. B* **1984,** *29,* 6443–6453.

(95) Finnis, M.W.; Sinclair, J.E. *Philos. Mag. A* **1984,** *50,* 45–55.

(96) Kim, S.G.; Horstemeyer, M.F.; Baskes, M.I.; Rais-Rohani, M.; Kim, S.; Jelinek, B.; Houze, J.; Moitra, A.; Liyanage, L. *J. Eng. Mater. Tech.* **2009,** *131,* 041210.

(97) Rudd, R.E. *Philos. Mag.* **2009,** *89,* 3133–3161.

(98) Han, S.; Zepeda-Ruiz, L.A.; Ackland, G.L.; Car, R.; Srolovitz, D.J. *J. Appl. Phys.* **2003,** *93,* 3328–3335.

(99) Biersack, J.P.; Ziegler, J.F. *Nucl. Instrum. Methods* **1982,** *194,* 93–100.

(100) Ackland, G.J.; Mendelev, M.I.; Srolovitz, D.J.; Han, S.; Barashev, A.V. *J. Phys.: Condens. Mater.* **2004,** *16,* S2629–S2642.

(101) Zepeda-Ruiz, L.A.; Han, S.; Srolovitz, D.J.; Car, R. *Phys. Rev. B* **2003,** *67,* 134114.

(102) Plimpton, S.J. *J. Comp. Phys.* **1995,** *117,* 1–19.

(103) Nosé, S. *J. Chem. Phys.* **1984,** *81,* 511–519.

(104) Hoover, W.G. *Phys. Rev. A* **1985,** *31,* 1695–1697.

(105) Parrinello, M.; Rahman, A. *Phys. Rev. Lett.* **1980,** *45,* 1196–1199.

(106) Zhou, M. *Proc. R. Soc. Lond. A* **2003,** *459,* 2347–2392.

(107) Li, J. *Modell. Simul. Mater. Sci. Eng.* **2003,** *11,* 173–177.

(108) Souidi, A.; Becquart, C.S.; Domain, C.; Terentyev, D.; Malerba, L.; Calder, A.F.; Bacon, D.J.; Stoller, R.E.; Osetsky, Yu.N.; Hou, M. *J. Nucl. Mater.* **2006,** *355,* 89–103.

(109) Han, S.; Zepeda-Ruiz, L.A.; Ackland, G.J.; Car, R.; Srolovitz, D.J. *Phys. Rev. B* **2002,** *66,* 220101.

(110) Zepeda-Ruiz, L.A.; Rottler, J.; Han, S.; Ackland, G.J.; Car, R.; Srolovitz, D.J. *Phys. Rev. B* **2004,** *70,* 060102.

(111) Zepeda-Ruiz, L.A.; Rottler, J.; Wirth, B.D.; Car, R.; Srolovitz, D.J. *Acta Mater.* **2005,** *53,* 1985–1994.

(112) Adams, J.B.; Foiles, S.M. *Phys. Rev. B* **1990,** *41,* 3316–3328.

(113) Ackland, G.J.; Thetford, R. *Philos. Mag. A* **1987,** *56,* 15–30.

(114) Rebonato, R.; Welch, D.O.; Hatcher, R.D.; Bilello, J.C. *Philos Mag A* **1987,** *55,* 655–667.

(115) Okuniewski, M.A.; Ashkenazy, Y.; Heuser, B.J.; Averback, R.S. *J. Appl. Phys.* **2004,** *96,* 4181–4188.

(116) Shiraishi, K.; Fukaya, K.; Katano, Y. *J. Appl. Phys.* **1974,** *54,* 275–285.

(117) Zinkle, S.J. *Phys. Plasmas* **2005,** *12,* 058101.